Supplement of Atmos. Meas. Tech., 13, 5319–5334, 2020
https://doi.org/10.5194/amt-13-5319-2020-supplement

Atmospheric Measurement Techniques
Open Access
EGU

Supplement of

Combining low-cost, surface-based aerosol monitors with size-resolved satellite data for air quality applications

Priyanka deSouza et al.

Correspondence to: Priyanka deSouza (desouzap@mit.edu)

S1. Dataset Details of the Nairobi Example

This section provides details of the MISR and MODIS satellite and OPC suborbital data collected for the Nairobi example, as well as the GEOS-Chem model input used to assess aerosol vertical distribution and composition.

S1.1. OPC-N2 deployment in Nairobi

On May 1, 2016, a team at the United Nations Environment Program (UNEP) deployed six low-cost PM monitors (Alphasense OPC-N2 models) in schools around Nairobi (deSouza, 2017). This was the first relatively long-term, continuous, *in situ* air quality monitoring project at multiple points around the city of multiple pollutants: NO_2, NO, SO_2, and PM. Ten months of PM data from five of the six Alphasense OPC-N2s deployed in Nairobi from May 2016 till March 2017 are used in this paper. In addition to PM estimates, these OPCs report the raw particle counts in 16 bins based on particle diameter, ranging from 0.38 μm to 17.5 μm (Table S1), The sampling flow rate logged by each OPC-N2 at each site varied between 3-8 ml/s, and the data integration period was constant at 5 seconds per sample for this deployment.

Each Alphasense OPC-N2 costs ~ US $450 (much less than the tens of thousands of dollars that reference air quality monitors cost). The monitors were deployed at Kibera Girls Soccer Academy (KGSA), located in the Kibera informal settlement near the railway; St Scholastica, situated ~20 meters away from the notoriously congested Thika highway, where we expected to capture pollution from vehicles; All Saints Cathedral School, close to Mbagathi road and several small shops and industries; UN Environment headquarters, located off UN Avenue in the relatively green area of Gigiri, and Alliance Girls School in Kikuyu, considered an urban background site (deSouza et al., 2017). A sixth monitor was deployed at the Viwandani Community Center in an informal settlement in the industrial area. However, due to an extended power outage, it did not log data after July 2016, so we do not use the data from this monitor in the current study. Note that some of the other monitors also experienced power-outages over shorter periods. The choice of these sites (Figure S1) was intended to allow us to measure the whole gamut of pollutant signatures from different sources in Nairobi. The monitors were mounted on walls at approximately 2 meters above the ground, close to adult breathing height, but out of reach of children, and protected from the rain with plastic shields (deSouza et al., 2017).

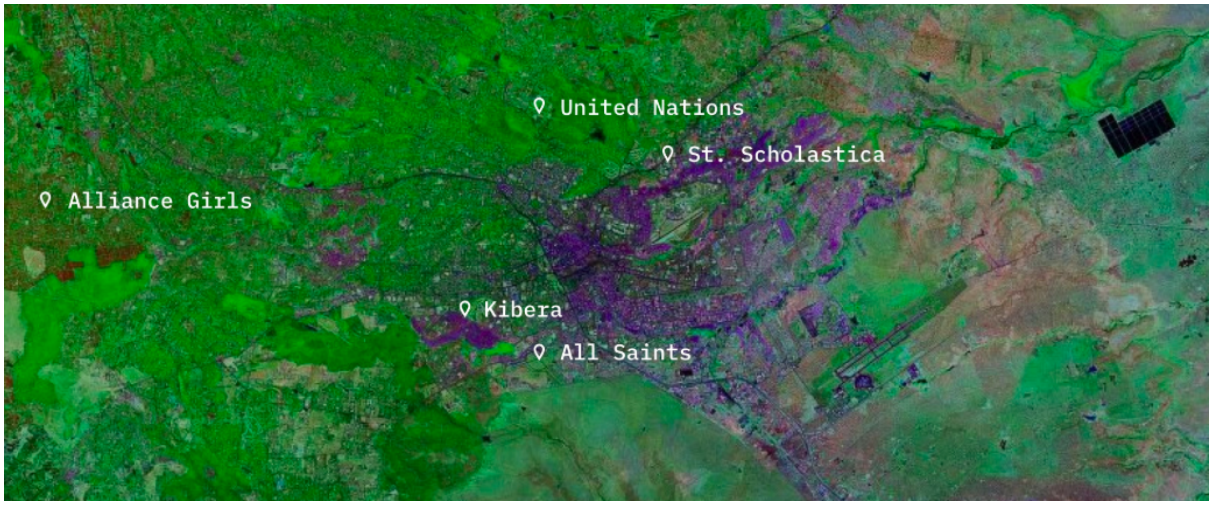

Figure S1: Image of the five deployment sites indicated by white stars. For scale, the distance between UNEP and St Scholastica is 5 km as the crow flies (© Google Maps)

Table S1: Minimum, maximum and center diameters for the 16 bins that the Alphasense OPC-N2 measures particle counts.

Bin number	Minimum Diameter (µm)	Maximum Diameter (µm)	Bin Center Diameter (µm)
1	0.38	0.54	0.46
2	0.54	0.78	0.66
3	0.78	1	0.89
4	1	1.3	1.15
5	1.3	1.6	1.45
6	1.6	2.1	1.85
7	2.1	3	2.55
8	3	4	3.5
9	4	5	4.5
10	5	6.5	5.75
11	6.5	8	7.25
12	8	10	9
13	10	12	11
14	12	14	13
15	14	16	15
16	16	17.5	16.75

Particle hygroscopicity is a consideration, as the OPCs operate at ambient relative humidity (RH), whereas $PM_{2.5}$ is assessed as dry mass. The Alphasense OPC-N2 sizing does depend on RH and aerosol hygroscopicity (Crilley et al., 2018; Hagan et al., 2019). However, the ambient average RH for the current study was 34% (Table S2); RH this low is unlikely to affect the OPC sizing. Further, previous studies (Gatari et al., 2005, 2009) found that organic carbon and black carbon dominate the urban air pollution particles in Nairobi, which are sourced from various types of combustion. The higher the amount of organic content, the less hygroscopic they tend to be (e.g., Samset et al., 2018). This means that the particles present are likely to have low hygroscopicity.

Figure S2 shows the derived $PM_{2.5}$ time series plots (in $\mu g/m^3$) for each Nairobi site from May 1 2016 to March 2 2017. PM data are recorded every minute. (The actual sampling time of the OPC-N2 is 5 seconds, after a 20 second warm-up period.) Some PM spikes registered are as high as 1000 $\mu g/m^3$. In order to smooth the time-series and

suppress outliers, that are likely due to instrument noise, we averaged the OPC measurements over 30-minute time intervals.

Co-locating the OPC with a reference monitor to obtain high-quality PM data would be required to calibrate the raw OPC measurements and distinguish the signal from noise directly. However, this would be costly and possibly time-consuming (Castell et al., 2017; Rai et al., 2017). Due to limited resources and lack of access to a reference monitor, we were unable to co-locate our low-cost sensors with a reference monitor in Nairobi. As such, we rely primarily upon the more robust raw particle counts per size bin reported by the monitors, rather than the reported $PM_{2.5}$.

Table S2: 30 minute-average dN/dln(D) (Units: #/ml) for Bins 2-7 from OPC surface measurements, coincident with the 10 favorable MISR retrievals, along with the daily-averaged temperature and relative-humidity. PM values are given in ($\mu g/m^3$).

date	orbit	site	temperature	relative humidity	PM_1	$PM_{2.5}$	PM_{10}	bin2	bin3	bin4	bin5	bin6	bin7
2016-08-02	88423	Alliance	28.7	35.1	6	9	26	8.2	5.0	2.1	1.2	1.1	0.6
2016-08-02	88423	UNEP	25.7	40.4	14	20	56	21.3	12.7	4.4	2.1	1.8	1.3
2016-10-14	89486	UNEP	28.9	35.8	11	19	71	18.4	14.9	6.0	3.7	3.0	2.2
2016-12-17	90418	UNEP	31.7	24.8	5	8	31	7.0	5.7	2.7	1.8	1.5	1.3
2016-08-02	88423	Scholastica	23.8	45.6	24	36	80	39.0	27.7	8.8	4.2	3.2	2.4
2016-10-14	89486	Scholastica	28.2	40.6	10	17	47	16.9	14.9	6.3	3.6	3.0	2.3
2016-08-02	88423	All Saints	26.7	39.9	6	9	25	9.2	6.6	2.8	1.3	1.2	0.8
2016-10-14	89486	All Saints	30.6	33.4	9	16	59	13.6	13.0	5.3	3.3	3.0	2.1
2016-08-02	88423	KGSA	27.3	41.4	11	18	71	18.8	13.7	4.8	2.4	2.4	2.0
2016-10-14	89486	KGSA	26.5	42.8	10	18	61	15.3	18.2	8.6	4.3	3.5	2.6

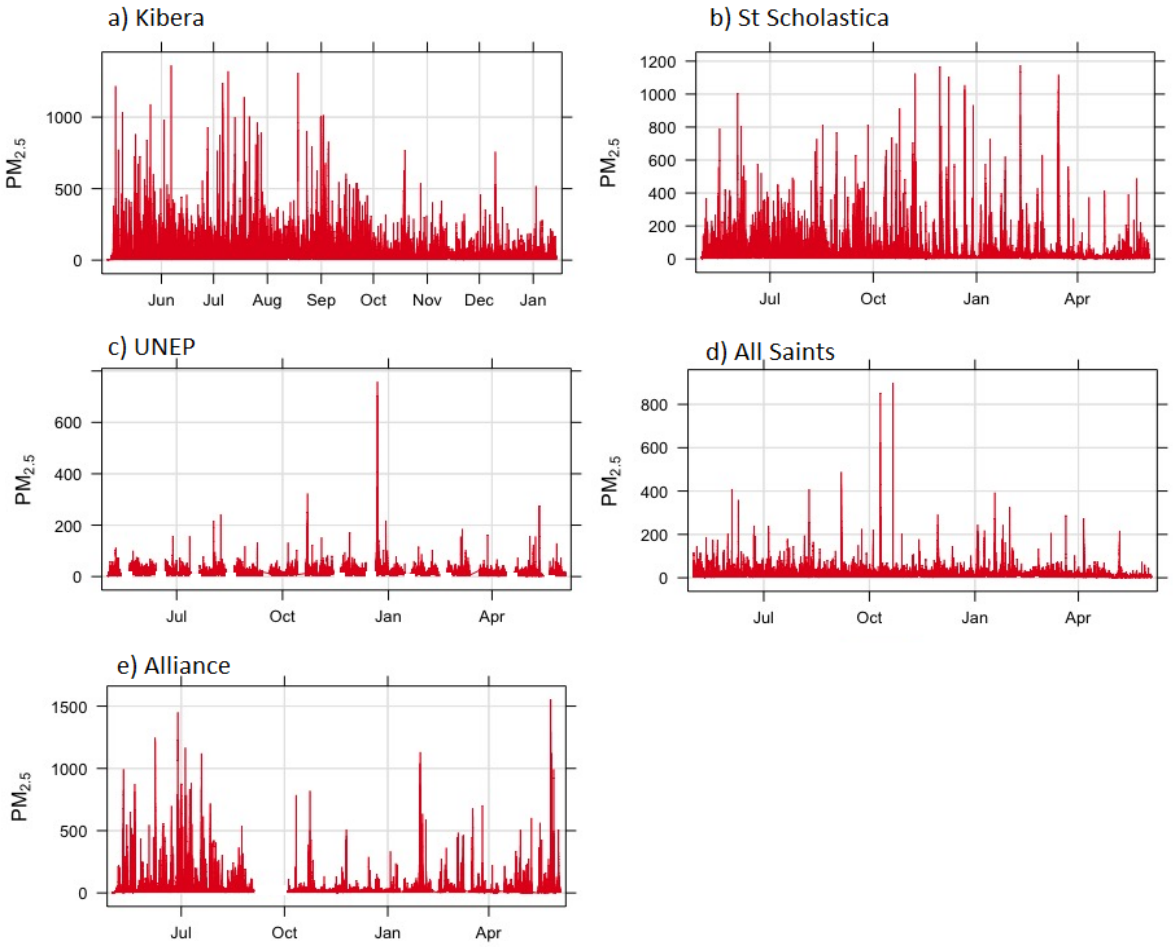

Figure S2: $PM_{2.5}$ (in $\mu g/m^3$) time-series plots for each of the five Nairobi deployment sites, from May 1, 2016 to March 2, 2017. There are gaps in the Alliance and UNEP plots because the monitors routinely lost electricity and thus did not make measurements during these periods.

S1.2. Satellite Data

S1.2.1. MISR Observations Over the Nairobi Sites

MISR Level 1B2 radiance data covering Nairobi from May 1 2016 to March 2 2017 were downloaded from the NASA Langley ASDC[1] for retrieval regions directly above each air quality monitoring site, and analyzed using the MISR Research Algorithm (RA; (Limbacher and Kahn, 2014; 2019) with the standard set of 74 mixtures. Each mixture is comprised of up to three of eight aerosol components (Kahn et al., 2010; Table S3). Separate MISR RA AOD retrievals, reported in the MISR green band (centered at 558 nm wavelength), were obtained for all eight MISR aerosol components (Table S3) for pixels within a radius of 1.6 km from each of the five Nairobi surface monitoring sites.

Over the course of the study period, we had only 28 successful MISR retrievals, during eight unique days. This is the main motivation for combining MISR retrievals with those of MODIS, as described below. The relatively low AOD over Nairobi during the study period makes estimating aerosol-type uncertainty difficult. We restricted the MISR

[1] https://eosweb.larc.nasa.gov/project/misr/mil2asae_table (Last accessed on August 12, 2019)

retrievals used in this study to the 10 that have total MISR AOD ≥ 0.15 (over three unique days), i.e., those meeting the good-quality MISR aerosol property criterion (Kahn et al., 2010).

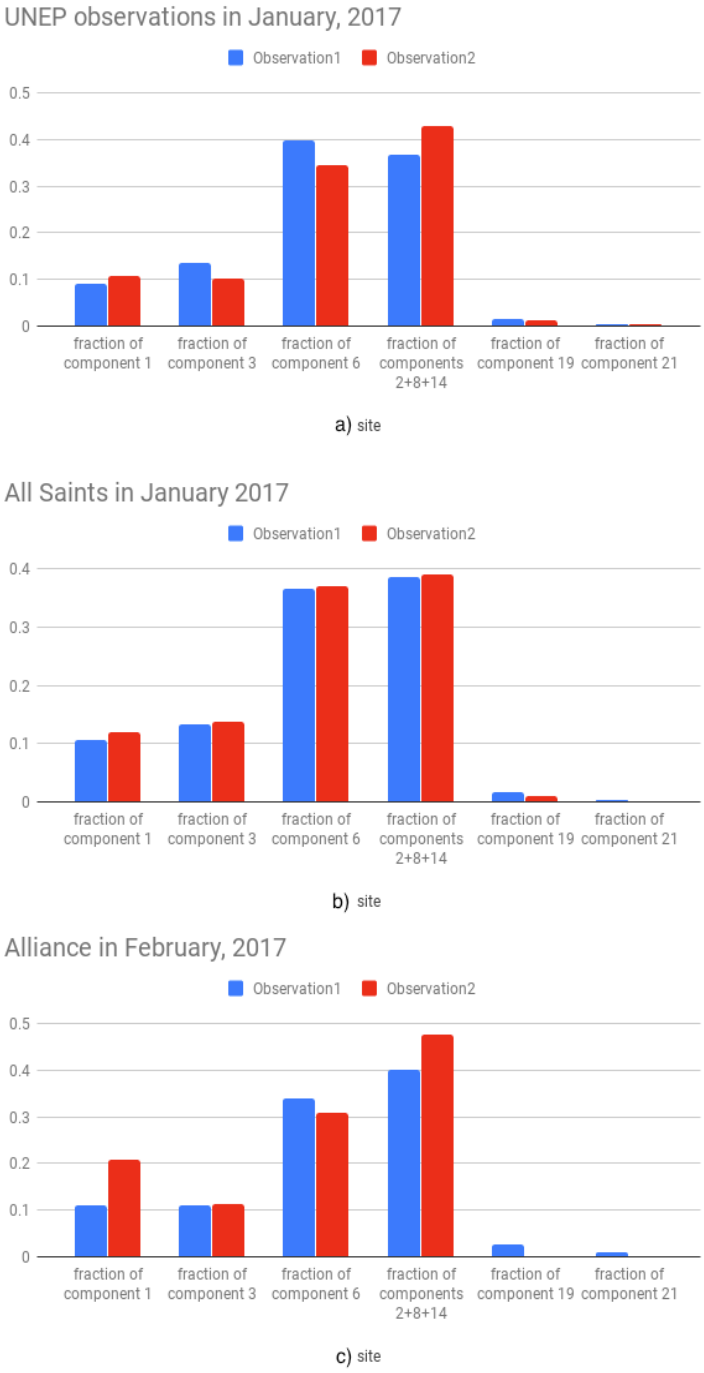

Figure S3: Examination of monthly particle-type variability for three cases where MISR obtained two retrievals at a given site in the same month. The fraction of the total near-surface AOD ($AOD_{N\text{-}S}$) ascribed to different MISR aerosol components is plotted for each case. Note that Components 2, 8, and 14 are aggregated, as discussed in Section 2.2.1 in the main text.

Unfortunately, we did not have multiple MISR observations with AOD ≥ 0.15 corresponding to a specific site in the same month. Therefore, we used the available MISR component AOD values obtained for a given site to represent

the 'monthly effective' particle size distribution for aerosols over that site. We excluded months when there were no MISR retrievals for a site. As such, we assume the fractional contributions of the near-surface MISR aerosol components to the total AOD remain nearly unchanged in the study region for a given month, even if the total AOD varies. We tested this assumption to some extent using all 28 MISR retrievals, as we do have several instances of two observations in a month over a specific site if we include the lower-AOD cases. Figure S3 shows the fractional AOD values for different MISR aerosol components where two observations over a specific site were made in the same month. It can be seen that the fractions are very similar, which lends some credence to our particle property assumption.

Table S3: Aerosol components assumed in MISR Research Algorithm for this study. This is the same component set as is used in the MISR Standard Algorithm, versions 22 and 23. For each aerosol component, Rc is the characteristic radius, σ is the distribution width of the lognormal size distribution, Re is the effective radius, and R1 and R2 are the minimum and maximum radii of the respective size distributions. The Spectral extinction coefficient represents the optical scattering + absorption of each aerosol component.

MISR component	**Component name**	**Particle size/Shape category**	**Rc (µm)**	**Re (µm)**	**σ**	**R1 (µm)**	**R2 (µm)**	**Spectral extinction coefficient (µm^2)**
1	Spherical_nonabsorbing_0.06	Small spherical	0.03	0.06	1.65	0.001	0.4	0.00039594
2	Spherical_nonabsorbing_0.12	Small spherical	0.06	0.12	1.7	0.001	0.75	0.013401464
3	Spherical_nonabsorbinb_0.26	Medium spherical	0.12	0.26	1.75	0.01	1.5	0.18231007
6	Spherical_nonabsorbing_2.8	Large spherical	0.5	2.8	1.9	0.1	50	16.189339
8	Spherical_absorbing_0.12_ssa_green_0.9	Small spherical, moderately absorbing	0.06	0.12	1.7	0.001	0.75	0.014069699
14	Spherical_absorbing_0.12_ssa_green_0.8	Small spherical, strongly absorbing	0.06	0.12	1.7	0.001	0.75	0.014874
19	Grains_mode1_h1 (dust)	Medium dust	0.5	0.21	1.5	0.1	1	3.168676
21	Grains_mode2_h1 (dust)	Coarse dust	1	3.32	2	0.1	6	15.51

Figure S4 shows the MISR columnar AOD for the 10 cases where the average total AOD ≥ 0.15. Small, spherical, light-absorbing (components: 8 and 14) and non-absorbing (component 2) particles are characteristic of organic aerosols and sulfate/nitrate, respectively (Kahn and Gaitley, 2015), and are typical of urban pollution particles. The component AOD values for these particle types are relatively high for all coincident observations, consistent with our expectation that local pollution dominates the aerosol loading in the Nairobi region (see Section S1.3 on the GEOS-

Chem model, below). Further, we know that the primary aerosol source in Nairobi during the study period is local pollution, so, lacking other constraints, assuming the particle type is constant on a monthly basis seems plausible. The AOD of component 6, a medium-large spherical particle often retrieved for dust, but also representing a generic large, spherical non-absorbing particle (Kahn and Gaitley, 2015), is moderately high for all coincident observations, especially for the five cases with the lowest overall AOD. This could be a transported aerosol, representing a background component, less likely to be concentrated near the surface. The AOD for component 21 is 0, implying this component was not present at a detectable level in any of the MISR retrievals considered. In light of limited MISR aerosol-type retrievals, the assumption of relatively constant aerosol-type fractions remains a limitation of the current study. Future experiments, performed farther away from the equator, will have more frequent MISR observations, and likely higher numbers of successful retrievals.

Figure S4: AOD for each MISR aerosol component retrieved from the Research Algorithm for the 10 coincident observations for which the total $AOD_{558} \geq 0.15$.

It takes about seven minutes for all 9 MISR cameras to observe a given location on the surface. We averaged the OPC $PM_{2.5}$ readings over 30 minutes, centered on the MISR overpass time. We matched these OPC values with the corresponding MISR RA AOD values for each component group, using a universe of 74 mixtures, within a radial distance of 1.6 km from each ground site. Each of the five sites has up to ~7 MISR RA coincidences within this radius. The MISR retrievals yielded a spatial distribution of spherical, light-absorbing and non-absorbing particles, with an effective radius of about 0.12 µm everywhere. Note that the size distribution for the 0.12 µm particles extends to 0.75 µm (Table S3); we rely on the tail of this distribution for comparisons with the OPCs, due to limited OPC sensitivity to smaller sizes.

S1.2.2. MAIAC/MODIS over Nairobi Sites

During the study period, the Terra satellite passed over Nairobi between ~10:30 am - 11:30 am local time. Aqua overpasses occurred approximately three hours after each Terra overpass. MAIAC AOD at 550 nm was extracted for

the study period from the Land Processes Distributed Active Archive Center (LP DAAC).[2] Although the MAIAC AOD at 550 nm is slightly more error-prone than that at 470 nm, we chose this AOD so it would be at essentially the same wavelength as the MISR-reported AOD. We selected only MAIAC AOD values where the cloud mask was 'clear' and the adjacency mask indicated that the adjacent pixel cloud masks were also clear. This led to a reduction of ~70% in the number of successful AOD retrievals, because Nairobi is at relatively high elevation and is often cloudy.

Hu et al. (2014) filled in the gaps of Terra AOD retrievals for different overpasses, when a successful Aqua AOD retrieval was obtained, and vice versa, using a simple linear regression. However, predicted AOD values inevitably contain additional uncertainties. Thus, we only used Terra AOD in this study. An additional advantage of working exclusively with Terra AOD is that MISR is also aboard Terra, so their observations are temporally coincident.

As with MISR, we matched the $PM_{2.5}$ reading of each OPC site with the corresponding MAIAC AOD values from the MODIS grid cells within a radial distance of 1.6 km, at Terra overpass time. We tested the robustness of our results to using radial distances of 1 km and 0.5 km. There were up to nine MAIAC grid cells linked with each site. As the KGSA and All Saints sites are 2.63 km apart, some of nine the grid cells associated with the two sites overlap.

The mean AOD of the 1712 successful Terra MAIAC retrievals is 0.095 (min=0.014, max=0.301, sd=0.053). The successful retrievals occur over 66 unique days. A total of 304 successful Terra MAIAC AOD retrievals were acquired, over 20 unique days, during months when favorable MISR retrievals (MISR AOD$\geq$ 0.15) were also obtained. Of these, 79 retrievals were made over UNEP, 48 were made over St Scholastica, 78 over KGSA, 87 over All Saints and 12 over Alliance. The mean successful Terra MAIAC AOD retrievals over these days is 0.126 (min=0.038, max=0.268, sd=0.048). We separately considered cases where the total MAIAC AOD $\geq$ 0.15 (85 of the 304 retrievals), in order to ensure that we were considering days when the surface aerosol dominated in the column.

S1.3. The GEOS-Chem Model

The GEOS-Chem model results are for 2012, the latest available, following two months of spin-up for chemical initialization, whereas the observations used in this paper are from 2016. Therefore, the model will underestimate any pollution sources that track population growth from 2012 to 2016. Population growth rates in Nairobi between 2012 and 2016 were ~8%; this is well within the GEOS-Chem model uncertainties, and given other uncertainties in the Nairobi example as well, we accept the 2012 estimates in the current analysis.

The GEOS-Chem model results indicate that the dominant aerosol components over Nairobi are organic aerosols (OA), typically produced from biofuel use (Figure S5). The model also shows negligible sulfate-nitrate-ammonium that is typical in most rapidly developing countries. The Nairobi low-cost sensor sites coincide with two GEOS-Chem grid cells. The UNEP site is in one cell, and the other sites are all in the other. The GEOS-Chem grid cells are of a different size compared with MISR grid cells, and we used the GEOS-Chem results for the non-UNEP sites only, as this cell has a maximum areal overlap with the corresponding MISR cell.

[2] https://lpdaac.usgs.gov/products/mcd19a2v006/ (Last accessed on June 12, 2019)

The fraction of AOD in the first layer of the GEOS-Chem model, as a proportion of the total-column AOD, provides the AOD vertical scaling factor (Figure S5). This factor is used to calculate the fractional AOD at the surface of Earth, to connect the near-surface aerosols mass results with the AOD from satellite data. The vertical scaling factors from GEOS-Chem, were ~ 0.4 for anthropogenic aerosol (SO_4, NO_3, OC and EC) and 0.07 for dust. We attempted to validate the GEOS-Chem-derived vertical scaling factor by comparing with statistical data from Cloud-Aerosol Lidar and Infrared Pathfinder (CALIPSO) L2 aerosol extinction coefficient retrievals for the same season over the Nairobi region. Unfortunately, the narrow CALIPSO swath (~100 meters) passes no closer than ~40 km from the urban center of Nairobi, making the AOD vertical scaling factor derived from the latter difficult to compare with that from GEOS-Chem. We nevertheless calculated the monthly-averaged vertical scaling from CALIPSO, by dividing the sum of the aerosol extinction coefficient at 532 nm for the near-surface aerosol layer by the sum of all the aerosol extinction coefficients for the entire column. For cells within ~100 km from the ground-based monitoring sites, the scaling factor varied between 0.1 and 0.2 over the months in 2016 for which we had MISR retrievals > 0.15. This is less than that from the GEOS-Chem grid cells, most likely because over rural areas, a larger fraction of aerosol in the column is transported, whereas the dominant aerosol in the urban center is locally sourced and concentrated nearer the surface.

We also attempted to evaluate this vertical scaling layer using the Cloud-Aerosol Transport System (CATS) instrument (on board the International Space Station) L2 particle backscatter coefficient at 1064 nm wavelength over the Nairobi region. The monthly-averaged vertical scaling from CATS reported for cells within ~ 50 km from the ground-based monitoring sites, calculated by dividing the sum of the particle backscatter coefficient at 1064 nm for the near-surface aerosol layer by the sum of all the particle backscatter coefficients for the entire column, varies between 0.01 and 0.2 over the months in 2016 for which we had MISR retrievals > 0.15. Unfortunately, the L2 CATS product does not contain information about the backscattering coefficient at or near 550 nm wavelength. The 1064 nm measurements are much less sensitive to the small sized urban particles and more likely weighted toward any transported soil or dust particles, making it difficult to compare the vertical scaling parameter from CATS with that from GEOS-Chem. However, GEOS-Chem has been validated at the regional scale (Marais et al., 2019), so we use the available vertical scaling parameters from the model.

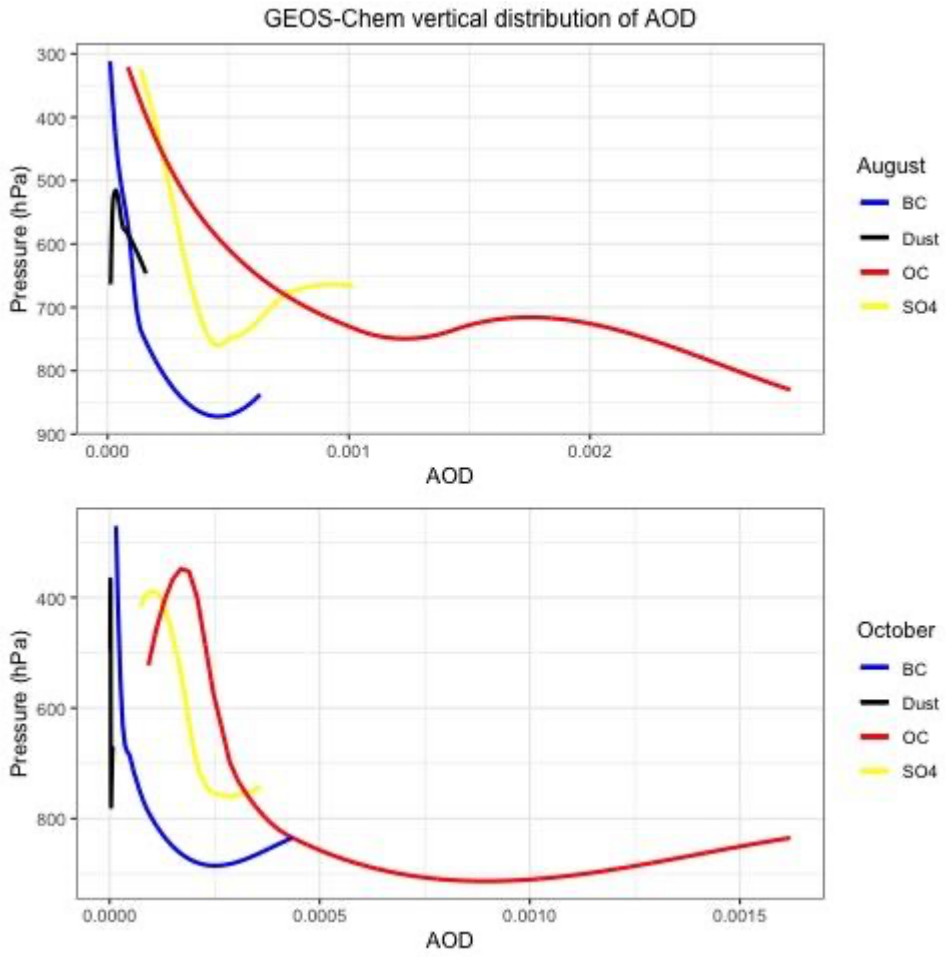

Figure S5: The vertical distribution of aerosol optical depth obtained from the GEOS-Chem model for October, for the model pixel above the UNEP site. Note: OA: Organic aerosols, BC: Black Carbon

The GEOS-Chem monthly scaling factors account for seasonal variation in the aerosol vertical distribution (Figure S5). However, as all of the ground-based sites fall within one GEOS-Chem grid cell, it does not account for any variation between sites in the local AOD-$PM_{2.5}$ relationships. In the ensuing analysis, we allowed for site-specific factors in our regression analysis to compare these relationships over the study area. For future deployments, local, direct measurements of vertical extinction or at least backscatter from lidar would reduce our reliance solely on model-simulated scaling coefficients. Also, having higher-spatial-resolution modeling would allow us to account for any variability on scales smaller than the ~200 km resolution of the GEOS-Chem simulations. One barrier to running the model at higher spatial resolution is the uncertainty in current emissions inventories, especially over much of the developing world.

S2. Details of the Nairobi Example Regression Analysis

Because the satellite data are stable and self-consistent, we explore how well the $PM_{2.5}$ reported by the OPCs track the variability in $AOD_{N\text{-}S}$ as estimated by MISR and by MAIAC.

We first ran a regression analysis to relate surface $PM_{2.5}$ to the total satellite MISR $AOD_{N\text{-}S}$ using Equation S1 for our 10 coincident readings, using the reported average $PM_{2.5}$ from the OPC-N2 network acquired over the 30 minutes around the Terra overpass time.

$$PM_{2.5} = \gamma \text{ x (total near-surface } AOD_{N\text{-}S}) \text{ (with no intercept)} \qquad \text{(S1)}$$

We obtained an adjusted R squared of 0.88, and a γ of 138.6 (95% Confidence Interval:107, 170.2). This high correlation indicates that the vertical scaling from GEOS-Chem works well for our sites. Note that when we ran Equation S1 using the column AOD instead of the near-surface component, we obtained an adjusted R squared of 0.89, which is comparable. This supports the assumption that the aerosol at our sites is concentrated near-surface.

Table 1 in Section 4 of the main text shows the total near-surface scaling of the MISR $AOD_{N\text{-}S}$ and the corresponding $PM_{2.5}$ (units: $\mu g/m^3$) for the ten cases where there are MISR RA retrievals over individual OPC sites in the Nairobi area, and the total-column mid-visible AOD exceeded 0.15.

We also scaled the MAIAC total-column AOD using the GEOS-Chem vertical distribution. We then ran simple linear regressions using the reported 30-minute-averaged $PM_{2.5}$ from the OPC-N2 network against the MAIAC $AOD_{N\text{-}S}$ in Equation S1. We had a total of 1712 coincident measurements MAIAC AOD and PM measurements over the course of this study.

We obtained an adjusted R squared of 0.66 and a γ of 170.7 (95% CI: 165.0, 176.5). Note, however, that when we restrict the AODs considered in the regression to retrievals where the total MAIAC AOD $\geq$ 0.15 (85 retrievals), i.e., when near-surface pollution likely dominates the total-column aerosol concentration, we obtain an adjusted R squared of 0.80 and a γ of 138.6 (95% CI: 130.7, 146.5).

When we considered site-specific effects and added a site-specific interaction term in the regression model i.e., using Equation S2 and all 1712 data points, we obtained an adjusted R squared of 0.68 and a γ_1 of 183.2 (95% CI: 167.0, 199.4) for the Alliance site, 141.4 (95% CI: 130.0, 152.7) for All Saints, 194.8 (95% CI: 181.8, 207.8) for Kibera Girls Soccer Academy, 207.7 (95% CI: 195.8, 219.6) for St Scholastica and 140.5 (95% CI: 128.8, 152.1) for UNEP. When we restricted the retrievals to those where the total MAIAC AOD $\geq$ 0.15, we obtained an adjusted R square of 0.85.

$$PM_{2.5} = \gamma_1 \text{ x site-specific-factor x AOD (excluding intercept terms)} \qquad \text{(S2)}$$

The lower R squared obtained with the MAIAC measurements using all 1712 measurements compared to MISR is probably because we used only a subset of MISR retrievals for which AOD $\geq$0.15, to ensure we were including only measurements for which the particle-type retrievals are likely of good quality. These are also cases where the near-surface aerosol likely dominates, favoring assumptions in our application. When we include the low-AOD MAIAC retrievals, noise from the land surface can contribute significantly to the satellite retrieval. In addition, small amounts of transported aerosol above the near-surface layer can introduce larger uncertainties to the analysis when the AOD is

low. When we restrict retrievals to total AOD >=0.15, we obtain a much closer correlation between the surface PM and MAIAC AOD retrievals as well.

Figure S6: AOD for each near-surface MISR aerosol component obtained from the 304 successful MAIAC retrievals.

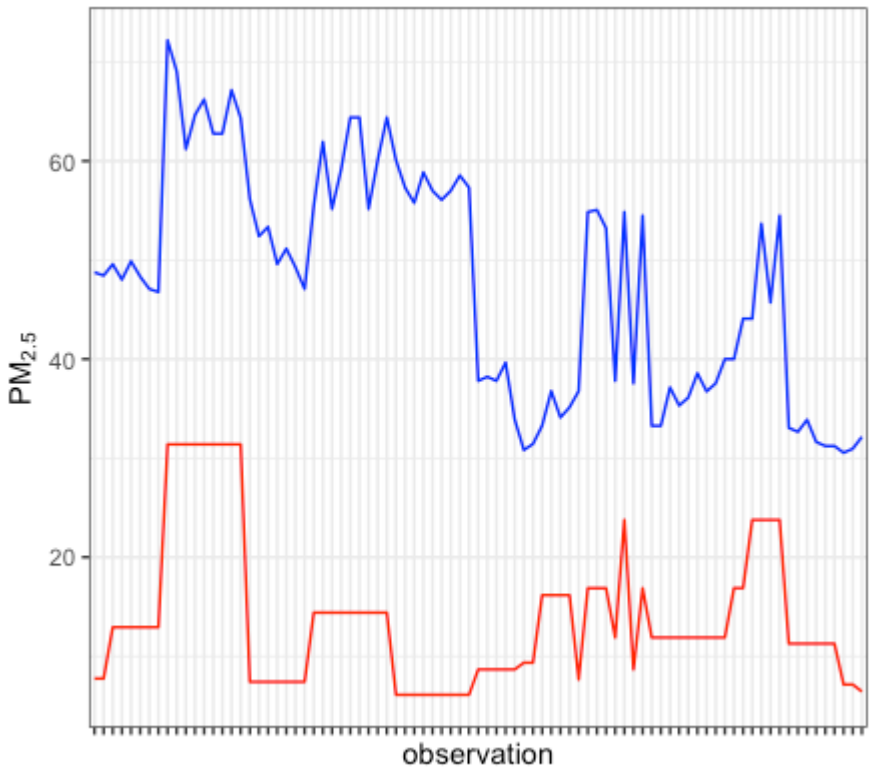

Figure S7: (Blue) $PM_{2.5}$ values (in $\mu g/m^3$) from the MAIAC Analysis 5 in Table 2. (Remember only 85 satellite observations with the total MAIAC AOD ≥ 0.15 are considered in this analysis.) The corresponding daily-averaged $PM_{2.5}$ from the ground-based OPC in units of $\mu g/m^3$ are shown in red. The correlation between the two estimates of PM is 0.47. Note that the flat estimates are because a single OPC $PM_{2.5}$ value was used to calibrate MAIAC AODs of the grid cells within a 1.6 km radius from each surface monitoring site. Thus, the same $PM_{2.5}$ value from an OPC is linked with multiple MAIAC-derived $PM_{2.5}$ concentrations.

References

Crilley, L.R., Shaw, M., Pound, R., Kramer, L.J., Price, R., Young, S., Lewis, A.C., Pope, F.D., 2018. Evaluation of a low-cost optical particle counter (Alphasense OPC-N2) for ambient air monitoring. Atmospheric Measurement Techniques 709–720.

deSouza, P., 2017. A Nairobi experiment in using low cost air quality monitors. Clean Air Journal 27, 12–42. https://doi.org/10.17159/2410-972X/2017/v27n2a6

Gatari, M., Wagner, A., Boman, J., 2005. Elemental composition of tropospheric aerosols in Hanoi, Vietnam and Nairobi, Kenya. Science of The Total Environment 341, 241–249. https://doi.org/10.1016/j.scitotenv.2004.09.031

Gatari, M.J., Boman, J., Wagner, A., 2009. Characterization of aerosol particles at an industrial background site in Nairobi, Kenya. X-Ray Spectrometry 38, 37–44. https://doi.org/10.1002/xrs.1097

Hagan, D.H., Gani, S., Bhandari, S., Patel, K., Habib, G., Apte, J.S., Hildebrandt Ruiz, L., Kroll, J.H., 2019. Inferring Aerosol Sources from Low-Cost Air Quality Sensor Measurements: A Case Study in Delhi, India. Environ. Sci. Technol. Lett. 6, 467–472. https://doi.org/10.1021/acs.estlett.9b00393

Kahn, R.A., Gaitley, B.J., 2015. An analysis of global aerosol type as retrieved by MISR. Journal of Geophysical Research: Atmospheres 120, 4248–4281. https://doi.org/10.1002/2015JD023322

Kahn, R.A., Gaitley, B.J., Garay, M.J., Diner, D.J., Eck, T.F., Smirnov, A., Holben, B.N., 2010. Multiangle Imaging SpectroRadiometer global aerosol product assessment by comparison with the Aerosol Robotic Network. Journal of Geophysical Research: Atmospheres 115. https://doi.org/10.1029/2010JD014601

Limbacher, J.A., Kahn, R.A., 2014. MISR Research Aerosol Algorithm: refinements for dark water retrievals. Atmospheric Measurement Techniques Discussions 7, 7837–7882. https://doi.org/10.5194/amtd-7-7837-2014

Limbacher, J.A. Kahn, R.A., 2019. Updated MISR Over-Water Research Aerosol Retrieval Algorithm - Part 2: A

Multi-Angle Aerosol Retrieval Algorithm for Shallow, Turbid, Oligotrophic, and Eutrophic Waters. Atmospheric Measurement Techniques 675–689. https://doi.org/10.5194/amt-12-675-2019, http://dx.doi.org/10.5194/amt-12-675-2019

Samset, B.H., Stjern, C.W., Andrews, E., Kahn, R.A., Myhre, G., Schulz, M., Schuster, G.L., 2018. Aerosol Absorption: Progress Towards Global and Regional Constraints. Curr Clim Change Rep 4, 65–83. https://doi.org/10.1007/s40641-018-0091-4